same equation with the DVFB control f given by Eq. (9) along with the sensor Eq. (8). The following stability result is obtained.

Theorem 1: The closed-loop system with DVFB is energy dissipative, i.e., $E(t)$ is decreasing, and if there are no zero frequencies in the open-loop system (i.e., Λ is positive definite) then the closed-loop system is stable for any $\xi \geq 0$ and asymptotically stable, if either 1) $\xi > 0$ or 2) $\xi \geq 0$ and $BQ^{1/2}$ is nonsingular.

Proof: From Eqs. (4) and (5),

$$E(t) = \tfrac{1}{2}(\dot{u}^T\dot{u} + u^T\Lambda u)$$

and, using Eq. (6),

$$\dot{E}(t) = \dot{u}^T\ddot{u} + \dot{u}^T\Lambda u = -2\xi\dot{u}^T\Lambda^{1/2}\dot{u} + \dot{u}^T Bf$$

But, from Eqs. (8) and (9),

$$f = -QB^T u$$

Therefore,

$$\dot{E}(t) = -\dot{u}^T[2\xi\Lambda^{1/2} + BQB^T]\dot{u}$$

However, $\Lambda^{1/2} \geq 0$ and $BQB^T \geq 0$, and so $\dot{E}(t) \leq 0$ or $E(t)$ is dissipative. If $\Lambda > 0$, then $E(t)$ is positive and $\dot{E}(t)$ is negative on all nonzero states $(u, \dot{u})$ and, consequently, $E(t)$ is a Lyapunov function.[4] Thus, the closed-loop system is stable, for any $\xi \geq 0$, and it is asymptotically stable if the matrix $W = 2\xi\Lambda^{1/2} + BQB^T$ is positive definite (i.e., $E(t)$ is decreasing). The matrix W is positive definite if either condition 1 or 2 is true and, therefore, the stability result is obtained.

The basic idea of Theorem 1 is well known in the mathematical literature on distributed parameter systems,[5] but does not seem to have penetrated the engineering literature on LSS. It should be noted that condition 2 of Theorem 1 is very difficult to achieve in practice because it requires that the number of sensors P equals the total number of modes L in the LSS. However, condition 1 is reasonable in that some damping is present in all LSS; the requirement that no rigid-body (zero frequency) modes be present can be alleviated partially by the following result.

Theorem 2: If Λ contains zero frequencies, where

$$\Lambda = \begin{bmatrix} 0 & 0 \\ 0 & \Lambda_2 \end{bmatrix} \qquad \Lambda_2 > 0$$

then a sufficient condition for stability of the nonzero frequency modes is that the energy in the zero frequency modes remains constant under feedback control (in particular, that the actuators do not excite the zero frequency modes). If the nonzero frequency modes are damped, then they are asymptotically stable.

Proof: Separate $E(t) = E_1(t) + E_2(t)$, where $E_1(t)$ is the energy in the zero frequency modes and $E_2(t)$ is the energy in the nonzero frequency modes. From Theorem 1, $\dot{E}(t) \leq 0$ or $\dot{E}_2(t) \leq -\dot{E}_1(t)$. Now, if $E_1(t)$ is constant, then $\dot{E}_2(t) \leq 0$ and, thus, $E_2(t)$ is a Lyapunov function for the nonzero frequency mode subsystem which makes it asymptotically stable. It is easy to see that $E_1(t)$ is constant for the special case where the actuators do not excite the zero frequency modes.

The important limitation of this result is that the energy in the rigid-body modes must be conserved while the controller is in operation; this can be achieved in some practical situations with actuators that do not excite rigid-body modes, e.g. member dampers, or with pairs of actuators where the rigid-body excitation is balanced out to zero. Nevertheless, DVFB must be used with care in LSS with any zero-frequency modes. It may be possible to introduce some position feedback control to shift the zero frequency modes away from zero; however, such feedback control alters the stiffness matrix Λ into a new $\bar{\Lambda}$ with no zero frequencies and this new $\bar{\Lambda}$ must be symmetric for the application of Theorem 1.

Finally, the choice of feedback gains Q needs to be addressed. Since Theorems 1 and 2 indicate stability regardless of the choice of Q (as long as Q is non-negative definite), the feedback gains become a design parameter. They can be chosen to improve the damping in any subset of critical vibration modes with the knowledge that the controller will not destabilize any part of the system (as long as the appropriate conditions of Theorems 1 or 2 are satisfied). However, the actual pole locations of the closed-loop system will have to be determined from a rather large symmetric eigenvalue calculation:

$$\det(s^2 + Ws + \Lambda) = 0 \tag{10}$$

where $W = 2\xi\Lambda^{1/2} + BQB^T$ and there are L conjugate pairs of poles.

Conclusions

DVFB does have limited application to LSS control; it can be used to supress vibrations in LSS under the following restrictions: 1) an equal number of collocated force actuators and velocity sensors are used; 2) the feedback gain matrix Q is non-negative definite; and 3) if zero frequency modes exist, the actuators must maintain constant energy in these modes (e.g., the actuators must not excite these modes). Under these restrictions, the DVFB controller cannot destabilize any part of the system no matter what the choice of feedback gains, and the stability margin of the closed-loop system will never fall below that of the open-loop system. However, the exact pole locations produced by DVFB must still be found from a large symmetric eigenvalue problem. This Note does not suggest that DVFB is suitable for the many other more complex LSS control problems, such as accurate pointing or attitude control, but it may prove useful as an adjunct to other controllers in dealing with the complex hierarchy and interdependence of LSS control problems.

References

[1] Balas, M., "Active Control of Flexible Structures," *Journal of Optimization Theory and Applications*, Vol. 25, July 1978, pp. 415-436.

[2] Skelton, R. and Likins, P., "Orthogonal Filters for Model Error Compensation in the Control of Nonrigid Spacecraft," *Journal of Guidance and Control*, Vol. 1, Jan.-Feb. 1978, pp. 41-49.

[3] Kato, T., *Perturbation Theory for Linear Operators*, Springer-Verlag, New York, 1966.

[4] LaSalle, J. and Lefschetz, S., *Stability by Lyapunov's Direct Method with Applications*, Academic Press, New York, 1961.

[5] Russell, D., "Linear Stabilization of the Linear Oscillator in Hilbert Space," *Journal of Mathematical Analysis and Applications*, Vol. 25, 1969, pp. 663-675.

Vector Methods in Homing Guidance

Malcolm J. Abzug*
Aeronautical Consultant, Pacific Palisades, Calif.

Nomenclature

$\boldsymbol{g}$	= acceleration of gravity
$\boldsymbol{i,j,k}$	= unit vectors along inertial reference axes
$\boldsymbol{n}$	= PN guidance load factor
$\boldsymbol{n_l}$	= PN load factor component due to line-of-sight rate
$\boldsymbol{R}$	= interceptor to target current range
$\boldsymbol{R_p}$	= predicted range vector

Received Jan. 5, 1979.

Index categories: LV/M Guidance; Guidance and Control.

*Fellow AIAA.

R_p^* = predicted closest approach range vector
t_f = time of flight
t_f^* = predicted time of flight to closest approach
V_r = interceptor velocity relative to the target
V_n = component of V_r normal to the range vector
x,y,z = components of range vector, inertial coordinates
$\dot{x},\dot{y},\dot{z}$ = components of relative velocity vector, inertial coordinates
λ = guidance gain
σ = angle between vectors V_r and R
ω = line-of-sight angular velocity

Introduction

HOMING guidance by proportional navigation (PN) is generally formulated in terms of line-of-sight rates measured by instruments mounted on a seeker head. Interceptor acceleration commands are calculated normal to the sensitive axes of the seeker-mounted instruments, allowing use of scalar PN laws for each such axis. This Note treats a more general case in which line-of-sight rate information is not necessarily available as the outputs of onboard instruments. Instead, target and interceptor parameters are given in inertial coordinates. This case, applicable to command homing guidance, requires a vector formulation of the PN law and other guidance results.

Vector PN Law

The usual planar or scalar formulation of the PN law is transformed into the following vector form:

$$n_I = \omega \times R\lambda V_r / gR \tag{1}$$

The cross-product operation of Eq. (1) generates a vector direction for the guidance load factor at right angles to the sight line (unit vector R/R) and angular velocity vectors, and in the correct direction to oppose line-of-sight rotation. The total PN command load factor n must account for gravity or

$$n = n_I - g/g \tag{2}$$

Line-of-Sight Angular Velocity

The interceptor vector velocity relative to the target V_r is obtained by subtracting the target velocity vector from the interceptor velocity vector. V_r is resolved into components along and normal to the range vector R. The normal component, called V_n, is in the plane of R and V_r. The line-of-sight angular velocity vector ω has the magnitude V_n/R and a direction normal to the R, V_r plane. These relationships are shown in Fig. 1. Now, the magnitude of V_n is $V_r \sin\sigma$ and the unit vector in the direction of ω is $V_r \times R / V_r R \sin\sigma$. Thus,

$$\omega = \frac{V_r \sin\sigma}{R} \frac{V_r \times R}{V_r R \sin\sigma} = \frac{V_r \times R}{R^2} \tag{3}$$

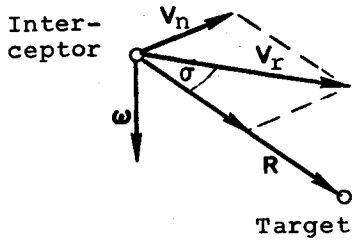

Fig. 1 Line-of-sight angular velocity.

PN Guidance Components

For use in guidance, the vector PN load factor commands of Eq. (2) must be resolved into components along interceptor body axes. However, the components of the vector quantities in Eqs. (1-3) are known in inertial coordinates. Thus, PN commands are first calculated in those axes. A coordinate transformation takes them to interceptor body axes. Inertial axes are assumed to be established by a ground-based tracking system or by initialization of onboard inertial instrument measurements. The required components in inertial axes are

$$\begin{aligned} R &= ix + jy + kz \\ V_r &= i\dot{x} + j\dot{y} + k\dot{z} \\ g &= kg \end{aligned} \tag{4}$$

Using these components in Eq. (3),

$$\begin{aligned} \omega_x &= (z\dot{y} - y\dot{z})/R^2 \\ \omega_y &= (x\dot{z} - z\dot{x})/R^2 \\ \omega_z &= (y\dot{x} - x\dot{y})/R^2 \end{aligned} \tag{5}$$

where

$$R = (x^2 + y^2 + z^2)^{1/2}$$

The PN load factor commands in inertial axes are

$$\begin{aligned} n = [\, & i(\omega_y z - \omega_z y) + j(\omega_z x - \omega_x z) \\ & + k(\omega_x y - \omega_y x)\,]\lambda V_r / Rg - k \end{aligned} \tag{6}$$

where

$$V_r = (\dot{x}^2 + \dot{y}^2 + \dot{z}^2)^{1/2} \tag{7}$$

The final step transforms the PN guidance load factor commands of Eq. (6) to body axes. The details of this step depend on the particular attitude coordinates used, such as Euler angles.

Predicted Miss Distance

Miss distance predictions can be made at any stage of an engagement by projecting current relative interceptor-to-target positions, velocities, and accelerations forward in time to the point of closest approach. Most practical purposes are served by a prediction based on positions and velocities only. This prediction becomes more precise as the remaining time approaches zero. The practical importance of miss distance

Table 1 Operation of miss distance predictor in end game

Time, s	Range, ft	Interceptor normal load factor	Interceptor lateral load factor	Target axial load factor	Predicted miss distance, ft
20.26	715.1	−15.0	−4.1	−46.2	11.1
20.28	383.8	−14.8	−1.8	−46.1	11.0
20.30	54.1	−14.3	1.4	−46.1	11.0
20.32	277.4	−13.8	5.9	−46.1	11.0

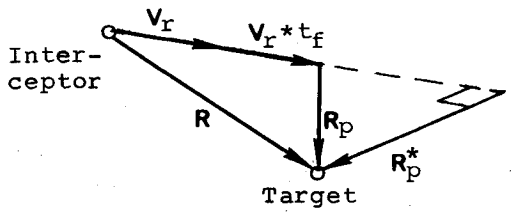

Fig. 2 Construction for predicted miss distance.

prediction is that more accurate measures of actual miss distance are obtained by projection than by interpolation from interceptor and target positions at discrete times. The required geometry is shown in Fig. 2. The predicted range vector $\boldsymbol{R}_p$ is found by projecting current positions and relative velocity $\boldsymbol{V}_r$ forward in time by t_f.

$$\boldsymbol{R}_p = \boldsymbol{R} - \boldsymbol{V}_r t_f \tag{8}$$

The minimum value of R_p or R_p^* is the closest approach. This occurs when the derivative of R_p^2 with respect to t_f vanishes. Squaring Eq. (8) gives

$$R_p^2 = R^2 - 2\boldsymbol{R}\cdot\boldsymbol{V}_r t_f + V_r^2 t_f^2$$

and

$$\partial R_p^2/\partial t_f = -2\boldsymbol{R}\cdot\boldsymbol{V}_r + 2V_r^2 t_f \tag{9}$$

setting Eq. (9) to zero

$$t_f^* = \boldsymbol{R}\cdot\boldsymbol{V}_r / V_r^2 \tag{10}$$

Using this result in Eq. (8), the predicted miss distance vector is

$$\boldsymbol{R}_p^* = \boldsymbol{R} - \boldsymbol{V}_r(\boldsymbol{R}\cdot\boldsymbol{V}_r)/V_r^2 \tag{11}$$

Equation (10) is easily reduced to components as

$$t_f^* = (x\dot{x} + y\dot{y} + z\dot{z})/(\dot{x}^2 + \dot{y}^2 + \dot{z}^2) \tag{12}$$

The predicted miss distance R_p^* is the length of the vector given in Eq. (11), found by taking the square root of the squares of the components of the right-hand side or

$$R_p^* = \left[\frac{(y\dot{x} - x\dot{y})^2 + (z\dot{y} - y\dot{z})^2 + (x\dot{z} - z\dot{x})^2}{\dot{x}^2 + \dot{y}^2 + \dot{z}^2}\right]^{1/2} \tag{13}$$

Numerical Example

Table 1 shows the end-game kinematics of a vehicle maneuvering under the PN law of Eq. (2) to intercept a reentry vehicle. At the last time point of 20.32 s, the interceptor has passed by the target and range is increasing. Average closing velocity is 16,500 fps. The minimum range point clearly cannot be found from the rapidly changing tabular values. On the other hand, the predicted miss distances from Eq. (13) are nearly constant at 11.0 ft. This is in the face of large and variable load factors.

Concluding Remarks

Proportional navigation for homing guidance is shown to have a vector formulation in addition to the classical scalar PN law. The vector formulation is suitable to the command guidance problem when line-of-sight rates can be deduced from interceptor and target positions and velocities in a set of inertial coordinates. Predicted miss distance derived from these same quantities converges satisfactorily in an interception at a high closing velocity.

Quaternion Singularity Revisited

Carl Grubin*
Northrop Corporation, Hawthorne, Calif.

Introduction

In a 1970 paper, Grubin[1] proposed an algorithm for extracting a quaternion from a given direction cosine matrix (DCM). The algorithm is relatively simple but is singular when the rotation angle is 180 deg. Recently, Klumpp[2] and Shepperd[3] have proposed algorithms that are singularity-free but more complex. The purpose of this Note is 1) to examine numerically the range of validity of Grubin's algorithm and demonstrate that it can be valid for rotation angles from 0 to 180 deg $-\epsilon$, where ϵ is as small as a few hundredths of a degree, and 2) propose an alternate algorithm for handling the singular case.

Analysis

Given a DCM that relates two rectangular frames, the problem is to extract the corresponding quaternion. Let the DCM elements be a_{ij} $(i,j=1,2,3)$. Equations (22) of Ref. 1 determine the quaternion elements ξ,η,ζ,χ as

$$\begin{aligned}\chi &= \cos(\theta/2) = (1+T)^{1/2}/2\\ \xi &= l\sin(\theta/2) = (a_{23}-a_{32})/4\chi\\ \eta &= m\sin(\theta/2) = (a_{31}-a_{13})/4\chi\\ \zeta &= n\sin(\theta/2)\,(a_{12}-a_{21})/4\chi\end{aligned} \tag{1}$$

where $T = a_{11}+a_{22}+a_{33}$. In Eqs. (1) l, m, n, θ are the Euler axis/angle as described in Ref. 1.

So long as χ is not too small, Eqs. (1) are valid expressions for ξ, η, ζ. The singularity occurs for $\chi\to 0$ $(T\to -1)$, corresponding to $\theta\to 180$ deg. However, whenever this occurs, simultaneously $a_{23}\to a_{32}$, $a_{31}\to a_{13}$, $a_{12}\to a_{21}$, so that ξ, η, $\zeta\to 0/0 = ?$ The question is, for what values of θ do Eqs. (1) begin to deteriorate?

Equations (7) and (19) of Ref. 1 give the DCM in terms of the Euler axis/angle parameters and the quaternion parameters, respectively. For the numerical studies, various sets of the Euler parameters were chosen, thereby generating values of the a_{ij}. The a_{ij} were then used in Eqs. (1) to determine the quaternion parameters. These, in turn, were substituted into Eqs. (19) of Ref. 1 to determine the reconstructed DCM elements $\hat{a}_{ij}$. The magnitude of the error

$$\epsilon_{ij} = |\hat{a}_{ij} - a_{ij}| \qquad (i,j=1,2,3)$$

was the quantity of interest.

Values of a switching angle, θ_s, were sought such that for $0\le\theta<\theta_s$ the errors would be "small." Also, for θ in the range $\theta_s\le\theta\le 180$ deg, alternate nonsingular expressions for ξ, η, ζ had to be developed. Ideally, θ_s should be such that maximum values for ϵ_{ij} would be equal for θ values slightly less than θ_s and slightly greater than θ_s.

Using a computer with 15-significant-figure accuracy and switching when $\chi = 2\times 10^{-4}$ gives $\theta_s = 179.9770817$ deg. Choosing θ slightly less, e.g., 179.9770807 deg and following the procedure described gave $\epsilon_{ij,\max} < 1\times 10^{-7}$. Again, choosing θ slightly greater than θ_s, e.g., 179.9770827 deg, and using the alternate expressions for ξ, η, ζ (given below), $\epsilon_{ij,\max}$ was again $<1\times 10^{-7}$. These results were verified for many

Received June 26, 1978; revision received Sept. 19, 1978.

Index categories: Spacecraft Dynamics and Control; Spacecraft Navigation, Guidance, and Flight-Path Control.

*Engineer Specialist, Electronics Division. Associate Fellow AIAA.